International Journal of Applied Engineering Research ISSN 0973-4562 Volume 13, Number 7 (2018) pp. 5554-5561

Dynamic Analysis of a Single MEMS Vibratory Gyroscope with Decoupling Connection between Driving Frame and Sensing Proof Mass

Vu Van The[1], Tran Quang Dung[1], Chu Duc Trinh[2]

[1] *Faculty of Mechanical Engineering, Le Quy Don Technical University, Hanoi, Vietnam.*
[2] *University of Engineering and Technology, Vietnam National University, Hanoi, Vietnam.*

Abstract

This paper reports a methodology to solve the dynamic analysis issue for micro-mechanical vibratory gyroscope with two mass elements which are connected by the U-shaped flexible beams. The equivalent stiffness coefficient of these beams is calculated by the analytical and simulation method with negligible error 3%. The differential motion equations of the gyroscope are set up and solved to determine the amplitude and phase of drive and sense modes formed analytical solution. The dimension of flexible beams is surveyed to achieve the suitable value of the desired mismatched resonant frequency as 100 Hz. The solution is compared with the results achieved by using ANSYS Workbench software with the different value 0.33%. The obtained results can be applied to mechanical structure design of MEMS vibratory gyroscope for optimizing the geometrical parameters and performance.

Keywords: mismatched frequency, decoupling connection, MEMS Vibratory Gyroscope, U-shaped beam.

INTRODUCTION

Micro-Electro-Mechanical Systems (MEMS) are generally considered as devices and systems integrated with mechanical elements, sensors, actuators, and electronic circuits on a common silicon substrate through micro-fabrication technology. In recent years, MEMS technology has been being developed owing to its advantages: small size, low power consumption, batch fabrication, low cost and ease of integration.

MEMS Vibratory Gyroscope (MVG) is a device used to detect and measure external angular velocity or rotational angle of an object relatively rotated in an inertial frame of reference [1], [2]. The operation of this sensor is based on the Coriolis principle to transform energy from primary mode to secondary mode [1÷5]. The MVGs have been extensively applied in the aerospace industry, automotive industry and consumer electronics market thanks to their dramatically reduced cost, size and weight [1÷8].

The MVGs are classified according to some factors such as the measured subject, the type of vibration, the number of mass element, the used effect for primary (drive) and secondary (sense) mode. There are two types of MVG which measures rotational angle for type I and angular rate for type II [4]. According to the effect used to create drive mode, the MVGs can be divided into some types: thermal drive [5], piezoelectric drive [6], electromagnetic drive [7] and electrostatic drive [8÷11]. Despite small productivity, the electrostatic effect is used more widely because of simple fabrication and control. The drive and sense vibration can be torsional vibration [9] or linear vibration [8] according to as the design in MVGs. Depending on the number of the mass element the MVGs can be classified into the single-mass or multi-mass gyroscope [12]. The advantages of the single-mass gyroscope are simple configuration and easy fabrication. This system operates as a resonator with the same frequency in drive and sense mode. However, at this frequency, the output signals are affected by the noise (disturbance to drive mode) coming from input angular velocity [8]. Besides, even small fabrication error, resulting in non-orthogonal elastic axes of the suspension beam may cause a serious error, when secondary motion appears not due to the external angular rate but is produced directly by the driving system via elastic cross-coupling [9÷11]. In order to overcome this problem, a decoupling frame is added as an element oscillating in driving direction to create the multi-mass gyroscope [13÷15]. This frame allows separating primary and secondary motions where the frame has been driven in the primary direction by exciting force and proof-mass is sense element in the secondary direction when applying an angular velocity in the direction perpendicularly to the primary and secondary direction (in-plane).

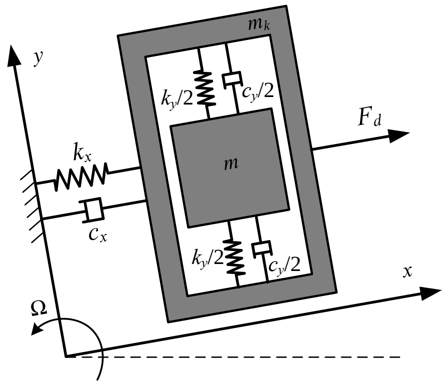

Figure 1: The schematic design of a MVG

Figure 1 shows a schematic design of a proposed MVG with a single proof-mass and a decoupling frame. It consists of a proof-mass m placed inside the outer frame m_k by the spring-damping suspension system. The frame is suspended by the flexible beams which are defined as a second spring-damping system. The flexible beams allow both the frame and the proof-mass to oscillate along the driving (x) direction. In addition, the proof-mass can move along the sensing (y) direction. In the driving direction, the frame and the proof-mass are driven into the resonant state by an external force with the suitable frequency. In this case, both the driving and sensing directions are in-plane while the out-of-plane angular rate is detected and measured. When the gyroscope is rotated with an angular rate Ω, a Coriolis force at the frequency of drive mode appears in the sense direction. This force induces the sense mode to the proof-mass in the sensing direction. This sense mode is detected and used to measure the angular rate. Thus, this vibratory gyroscope is presumed to the 2-degree-of-freedom system with two linear oscillations in two orthogonal directions.

In this type of MVG, the important problem is to determine the mismatched resonant frequency of the drive and sense modes. It is a major parameter for increasing the sensitivity of gyroscope due to increasing the mechanical quality factor of sense mode [13÷15]. In designing process of MVGs, it is necessary to solve the problem by the analytical and simulation method to reduce expenditure before fabrication. In addition, the tuning fork gyroscopes which consist of two identical tines are being studied in present to increase the performance of the devices. In their configuration, each tine is defined as a single gyroscope with two masses or more connected by decoupling beams. They are linked directly or indirectly to each other by a mechanism [16], [17]. So, the single gyroscope with two masses with decoupling connected beam need to be studied seriously. Each above gyroscope is defined as a resonator with the close frequency between drive and sense modes. This difference frequency is therefore called the mismatched frequency. It is one of the most important parameters to assess the performance of the MVGs.

This paper presents a methodology to determine the resonant frequency including the driving and sensing frequency of a single MVG. Hence, the suitable mismatched frequency between drive and sense mode is determine. This methodology allows to carry out the optimal dimension parameters of the desired single MVG to obtain the expected mismatched frequency. The solution is achieved by using both numerical analytical and simulated method. This proposed methodology is then used to design a silicon single MVG with a two-degree-of-freedom gyroscope. In this gyroscope structure, the sensing mass and out driving frame are connected together by using U-shaped flexible beams.

CONFIGURATION OF PROPOSED MVG

The configuration of proposed MVG is created in ANSYS Workbench and shown in Figure 2a. It has one proof-mass (1) which is suspended on an outer frame (2) thanks to four elastic beams (3). The frame is suspended on a substrate (not shown in Figure 2a) by four other elastic beams (4). The elastic beams (3, 4) have a U-shaped form with a fixed end and the guided other end. The three-dimensional (3D) solid model (Figure 2a) does not include the etch holes on the proof-mass and comb finger in drive and sense directions. When the driving signals are present, the outer frame and the proof-mass oscillate along the *x*-axis (drive axis); additionally the proof-mass oscillates along the *y*-axis (sense axis) when the gyroscope is effected by Ω angular rate (in the *z*-axis). This MVG is defined as single mass with decoupling frame system.

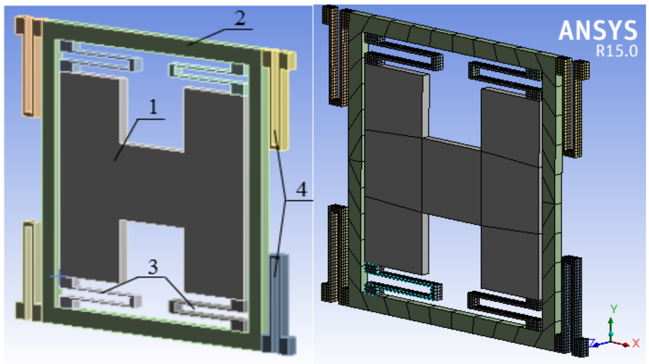

a) The 3D solid model b) The mesh model

Figure 2: 3D schematic design of a single MVG

The specific material parameters of Silicon are shown in Table 1. The dimensions of MVG are listed in Table 2.

Table 1: Properties parameters of Silicon

Property	Value	Unit
Density	2230	kg/m^3
Poisson's ratio	0.28	1
Young's modulus	169×10^9	Pa
Bulk modulus	1.2879×10^5	Pa

Table 2: The dimensions of the proposed MVG

Design parameter	Value
Dimensions of MVG ($x \times y$)	2240 × 1930 µm
Thickness of structure	60 µm
Surface area of the proof-mass	15468×10^2 µm^2
Surface area of the outer frame	7678×10^2 µm^2
Length of the drive springs	500 µm
Width of the drive springs	20 µm
Length of the sense springs	460 µm
Width of the sense springs	16 µm
Mass of the outer frame	1.0734×10^{-7} kg
Sensing mass	2.1624×10^{-7} kg
Sensing spring mass	4.8231×10^{-9} kg
Driving spring mass	5.578×10^{-9} kg
Gyroscope total mass	3.6518×10^{-7} kg

The equivalent stiffness coefficients of the driving and sensing spring beams are determined by James J. Allen [18] as follow:

$$K_x = \frac{Eh}{4}\left(\frac{b}{L}\right)^3\left(\frac{L'b^3 + 2Lb'^3}{2L'b^3 + Lb'^3}\right) \tag{1}$$

In the above expression, K_x is equivalent stiffness coefficient of a folded beam in x-direction; E is Young's modulus of Silicon; L, L', b, b' is the length, width of a folded beam and h is the thickness of structure (Figure 3).

Besides, the stiffness coefficients could be calculated by using simulation software ANSYS Workbench. The value of equivalent stiffness coefficient of one folded beam in driving direction is determined and shown in Figure 4.

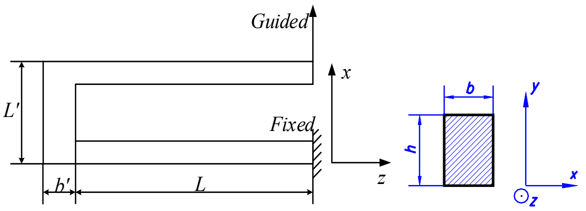

Figure 3: The U shaped folded beam

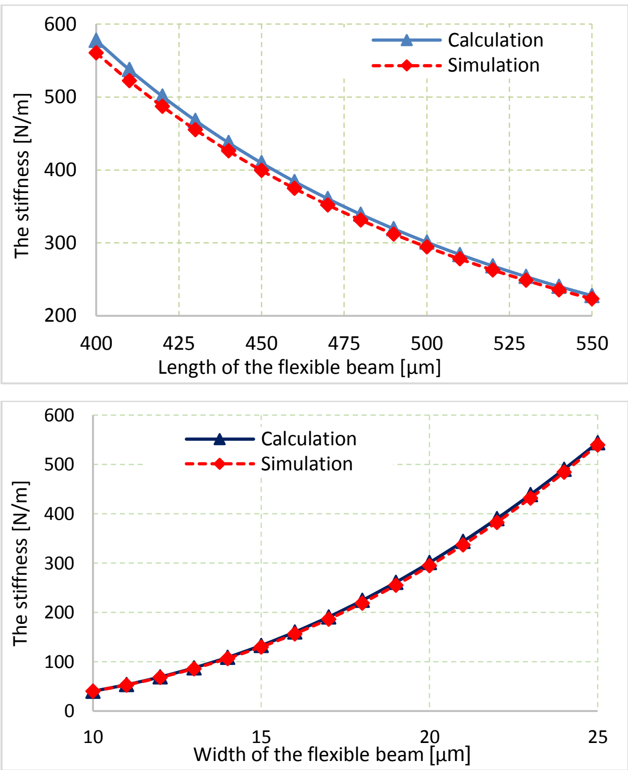

Figure 4: The dependence of the stiffness on parameters of the flexible beam

The results demonstrate that the value of the stiffness in two cases is slightly different (3%). Then the stiffness coefficients for a single folded beam in driving (k'_d) and sensing (k'_s) directions are respectively as:

$$k'_d = 294 \text{ N/m}; \ k'_s = 198 \text{ N/m}$$

Therefore, the equivalent stiffness coefficient in driving (k_x) and sensing (k_y) directions for the whole system are:

$$k_x = 4k'_d = 1176 \text{ N/m}; \ k_y = 4k'_s = 792 \text{ N/m}$$

These coefficients are used to find out the analytical solution of dynamic problem mentioned in previous section.

ANALYTICAL SOLUTION

Considering in the non-inertial reference frame $Oxyz$ with origin at the gravity center of the proof-mass where Ox, Oy and Oz axes are representative of driving, sensing and angular velocity direction, the differential motion equations of system are obtained by using Lagrange equation of the second kind [19]. The position of gravity center of decoupling frame is given by a vector $\vec{r}_k = \{x, 0, 0\}$, while the vector $\vec{r} = \{x, y, 0\}$ defines the position of the gravity center of the proof-mass. In common case, the angular velocity vector $\vec{\Omega}$ is defined by its projections on the reference frame as a vector $\vec{\Omega} = \{\Omega_x, \Omega_y, \Omega_z\}$. The absolute velocities of the frame $\vec{V}_k$ and the proof-mass $\vec{V}$ are defined by following expressions:

$$\begin{aligned} \vec{V}_k &= \dot{\vec{r}}_k + \vec{\Omega} \wedge \vec{r}_k = \{\dot{x},\ x\Omega_z,\ -x\Omega_y\} \\ \vec{V} &= \dot{\vec{r}} + \vec{\Omega} \wedge \vec{r} = \{\dot{x} - y\Omega_z,\ \dot{y} + x\Omega_z,\ y\Omega_x - x\Omega_y\} \end{aligned} \tag{2}$$

Total kinetic energy of the system will be presented as following expression:

$$\begin{aligned} T &= \frac{m_k}{2}\vec{V}_k^2 + \frac{m}{2}\vec{V}^2 \\ &= \frac{m_k}{2}\left[\dot{x}^2 + x^2\Omega_z^2 + x^2\Omega_y^2\right] + \\ &+ \frac{m}{2}\left[(\dot{x} - y\Omega_z)^2 + (\dot{y} + x\Omega_z)^2 + (y\Omega_x - x\Omega_y)^2\right] \end{aligned} \tag{3}$$

Total potential energy of the springs in the flexible suspension of the system will be presented as following expression:

$$\Pi = \frac{k_x}{2}x^2 + \frac{k_y}{2}y^2 \tag{4}$$

where k_x and k_y is equivalent stiffness of the flexible beams in drive and sense direction, respectively.

Total dissipative energy of the damping element in the suspension system can be expressed as:

$$\Phi = \frac{c_x}{2}\dot{x}^2 + \frac{c_y}{2}\dot{y}^2 \tag{5}$$

where c_x and c_y is equivalent damping coefficient of the system in driving and sensing direction, respectively.

Lagrange equation of the second kind for this system is given by:

$$\frac{d}{dt}\left(\frac{\partial L}{\partial \dot{q}_i}\right)+\frac{\partial \Phi}{\partial \dot{q}_i}-\frac{\partial L}{\partial q_i}=Q_i \quad (i = 1, 2) \tag{6}$$

Here L = T – Π is the Lagrange function, Q_i are generalized forces acting on the elements.

Combining expressions (3), (4) and (5) into the Lagrange function (6), simplifying gives us the following system of two differential equations, describing the motion of the MVG system:

$$\begin{cases}(m+m_k)\ddot{x}+c_x\dot{x}+\left[k_x-(m+m_k)(\Omega_y^2+\Omega_z^2)\right]x- \\ \quad -2m\Omega_z\dot{y}+m(\Omega_x\Omega_y-\dot{\Omega}_z)y=Q_1 \\ m\ddot{y}+c_y\dot{y}+\left[k_y-m(\Omega_x^2+\Omega_z^2)\right]y+2m\Omega_z\dot{x}+ \\ \quad +m(\Omega_x\Omega_y+\dot{\Omega}_z)x=Q_2\end{cases} \tag{7}$$

These equations can be rewritten by dividing both parts of the equations by corresponding coefficients (m + m_k for the first equation and m for the second one). The result is as following form:

$$\begin{cases}\ddot{x}+2\mu_x\dot{x}+\left[\omega_x^2-(\Omega_y^2+\Omega_z^2)\right]x-2d\Omega_z\dot{y}+d(\Omega_x\Omega_y-\dot{\Omega}_z)y=a_1 \\ \ddot{y}+2\mu_y\dot{y}+\left[\omega_y^2-(\Omega_x^2+\Omega_z^2)\right]y+2\Omega_z\dot{x}+(\Omega_x\Omega_y+\dot{\Omega}_z)x=a_2\end{cases} \tag{8}$$

where $\omega_x^2=k_x/(m+m_k)$ and $\omega_y^2=k_y/m$ are natural frequencies of drive and sense mode, $d=m/(m+m_k)$ is dimensionless inertia asymmetry factor (d = 1, equation system (8) becomes motion equations for the single mass MVG without decoupling frame), $a_1=Q_1/(m+m_k)$ and $a_2=Q_2/m$ are generalized accelerations from external forces, $\mu_x=c_x/2(m+m_k)$ and $\mu_y=c_y/2m$ are damping factors in the drive and sense direction, respectively.

The components of the angular velocity (include Ω_x and Ω_y) cause any displacement of proof mass in motion plane. It is only Ω_z in terms of Coriolis forces ($2m\Omega_z\dot{x}$ and $2m\Omega_z\dot{y}$ in equations (7)) that cause the translation energy between two oscillations in-plane. Therefore, in general case, the vector angular velocity can be assumed as they are constants or quasi-constants and defined by the simpler form as $\vec{\Omega}=\{0,0,\Omega\}$. The equation system (8) can be rewritten as:

$$\begin{cases}\ddot{x}+2\mu_x\dot{x}+(\omega_x^2-\Omega^2)x-2d\Omega\dot{y}=a_1 \\ \ddot{y}+2\mu_y\dot{y}+(\omega_y^2-\Omega^2)y+2\Omega\dot{x}=a_2\end{cases} \tag{9}$$

In this MVG model, the external forces apply on the elements including electrostatic force in drive direction ($\vec{F}_d$ in x-direction), the system (8) can be simplified as:

$$\begin{cases}\ddot{x}+2\mu_x\dot{x}+(\omega_x^2-\Omega^2)x-2d\Omega\dot{y}=a_d \\ \ddot{y}+2\mu_y\dot{y}+(\omega_y^2-\Omega^2)y+2\Omega\dot{x}=0\end{cases} \tag{10}$$

where $a_d=F_d/(m+m_k)$ is generalized acceleration from the drive force.

If exciting force of the drive oscillation is harmonic with the form as $a_d=\mathrm{Re}\{ae^{i\omega t}\}$ where ω is the exciting frequency and initial phase is assumed as zero, the solutions of system (10) can be determined by using Kramer's method with assumed form for harmonic oscillation of the elements as:

$$\begin{matrix} x(t)=\mathrm{Re}\{A_1e^{i\omega t}\} & A_1=A_{10}e^{i\varphi_{10}} \\ y(t)=\mathrm{Re}\{A_2e^{i\omega t}\} & A_2=A_{20}e^{i\varphi_{20}}\end{matrix} \tag{11}$$

where A_{10}, A_{20} and φ_{10}, φ_{20} are amplitudes and initial phases of the drive and sense oscillation, respectively. The equations which express the relation of the amplitudes are written as following:

$$\begin{cases}(\omega_x^2-\Omega^2-\omega^2+2\mu_x\omega i)A_1-2d\Omega\omega iA_2=a \\ 2\Omega\omega iA_1+(\omega_y^2-\Omega^2-\omega^2+2\mu_y\omega i)A_2=0\end{cases} \tag{12}$$

The solution of the system (12) is:

$$A_1=\frac{a(\omega_y^2-\Omega^2-\omega^2+2\mu_y\omega i)}{\bar{\Delta}};\ A_2=\frac{2a\Omega\omega i}{\bar{\Delta}} \tag{13}$$

where

$$\bar{\Delta}=(\omega_x^2-\Omega^2-\omega^2)(\omega_y^2-\Omega^2-\omega^2)-4\omega^2(d\Omega^2+\mu_x\mu_y)+ \\ +2\omega\left[\mu_x(\omega_y^2-\Omega^2-\omega^2)+\mu_y(\omega_x^2-\Omega^2-\omega^2)\right]i$$

The value of amplitude and phase of oscillations can be determined by following:

$$\begin{aligned}A_{i0}&=|A_i|=\sqrt{\mathrm{Re}(A_i)^2+\mathrm{Im}(A_i)^2} \\ \varphi_{i0}&=\tan^{-1}\left(\frac{\mathrm{Im}(A_i)}{\mathrm{Re}(A_i)}\right)\end{aligned} \quad (i = 1, 2) \tag{14}$$

Therefore, the expressions for amplitude and phase are:

$$A_{10}=\frac{a\sqrt{(\omega_y^2-\Omega^2-\omega^2)^2+4\mu_y^2\omega^2}}{\Delta};\ A_{20}=\frac{2a\Omega\omega}{\Delta} \tag{15}$$

$$\begin{aligned}\varphi_{10}&=\tan^{-1}\left(\frac{2\omega\left[\mu_xB_1-(\omega_x^2-\Omega^2-\omega^2)B_2\right]}{(\omega_x^2-\Omega^2-\omega^2)B_1+4\mu_x\omega^2B_2}\right) \\ \varphi_{20}&=\tan^{-1}\left(B_1/2\omega B_2\right)\end{aligned} \tag{16}$$

where

$$\Delta^2=\left[(\omega_x^2-\Omega^2-\omega^2)(\omega_y^2-\Omega^2-\omega^2)-4\omega^2(d\Omega^2+\mu_x\mu_y)\right]^2+ \\ +4\omega^2\left[\mu_x(\omega_y^2-\Omega^2-\omega^2)+\mu_y(\omega_x^2-\Omega^2-\omega^2)\right]^2$$

$$B_1=(\omega_x^2-\Omega^2-\omega^2)(\omega_y^2-\Omega^2-\omega^2)-4\omega^2(d\Omega^2+\mu_x\mu_y)$$
$$B_2=\mu_x(\omega_y^2-\Omega^2-\omega^2)+\mu_y(\omega_x^2-\Omega^2-\omega^2)$$

The expressions (15), (16) represent the amplitude and phase of drive and sense oscillation as the functions of both excited frequency and angular velocity. These relations are shown in Figures 5 and 6.

One can observe that the sensing amplitude is proportional to angular velocity. This relation is linear when the angular velocity is small enough (under 100 rad/s) and the driving amplitude is quasi-constant. Besides, the driving and sensing frequencies change insignificantly and the mismatched frequency between driving and sensing modes is constant. By increasing the angular velocity the sensing and driving amplitudes and the mismatched frequency increase nonlinearly. This characteristic allows to determine the measuring range of the MVG.

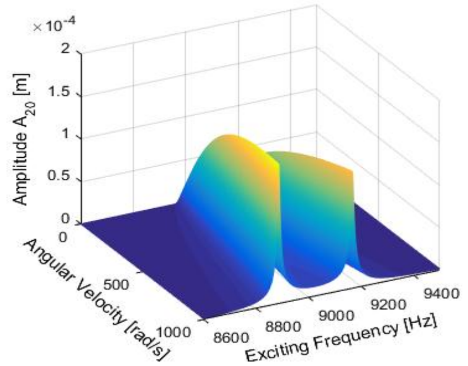

a) ISO view

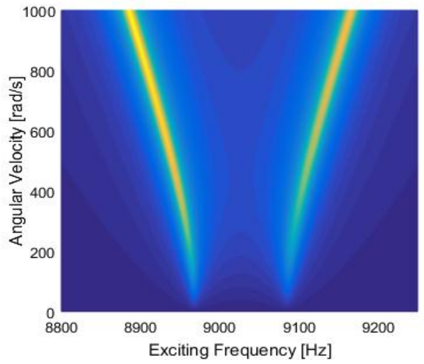

b) Top view

Figure 5: The dependence of sensing amplitude on exciting frequency and angular velocity

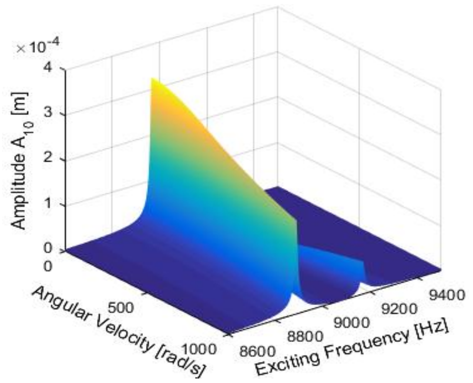

a) ISO view

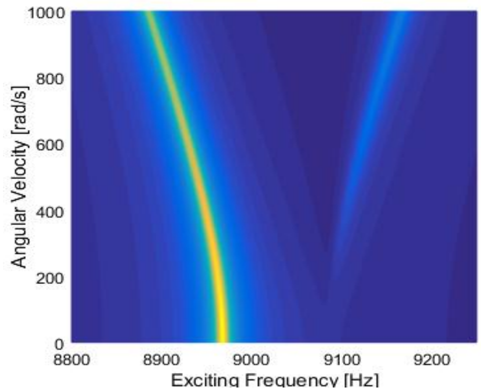

b) Top view

Figure 6: The dependence of driving amplitude on exciting frequency and angular velocity

FEM ANALYSIS

In this paper, the ANSYS Workbench is used to create, analyze and simulate the proposed model in Figure 2a. The mesh model for beams are controlled by using element size of 20 µm, whereas the rest of this MVG is defined by using maple face meshing with element size of 400 µm and 600 µm to reduce element quantity. The finite element type in this model is SOLID 187 (element 3D with 10 nudes). The element quantity for MVG is 9133. The MVG after mesh is shown in Figure 2b.

The fundamental motion equation of system is defined as:

$$[M]\{\ddot{u}\}+[C]\{\dot{u}\}+[K]\{u\}=\{P_{ex}\} \qquad (17)$$

where $[M]$ - the mass matrix; $[C]$ - the damping matrix; $[K]$ - the spring matrix; $\{u\}$ - the displacement vector and $\{P_{ex}\}$ - the external force vector.

In MEMS devices, the viscous effects of the air between the masses and the substrate are discussed. The damping coefficients are defined to Rayleigh function [20]:

$$[C] = \alpha[M] + \beta[K] \qquad (18)$$

where α and β are the Rayleigh damping coefficients and defined as constants.

Modal analysis

It is important to find out the desired resonant frequencies, where the displacement of the proof-mass in driving and sensing directions is maximum.

In general, this structure needs to have some advantages. First of all, the drive and sense modes should be appeared before the other ones. The drive and sense modes are major modes, whereas the others are parasitic modes. These major frequencies should be far different from the parasitic ones [13÷17]. The modal analysis is carried out to determine the natural frequencies of structures by solving equation (1) without external force. Six frequencies of the proposed MVG are shown in Table 3. Some natural frequencies of this MVG are shown in Figure 7.

Table 3: Six vibratory modes of the proposed MVG

Vibratory modes	Frequency (Hz)
Drive mode	8757
Sense mode	9095
Third mode	12799
Fourth mode	18688
Fifth mode	19487
Sixth mode	27729

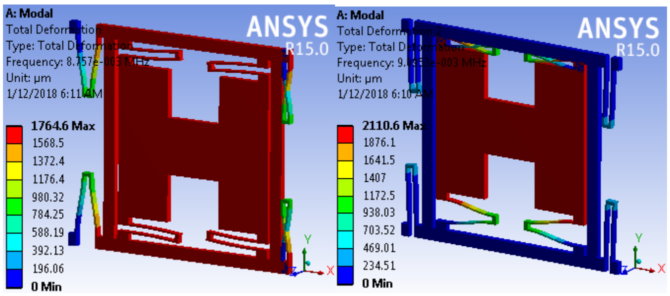

a) The drive mode b) The sense mode

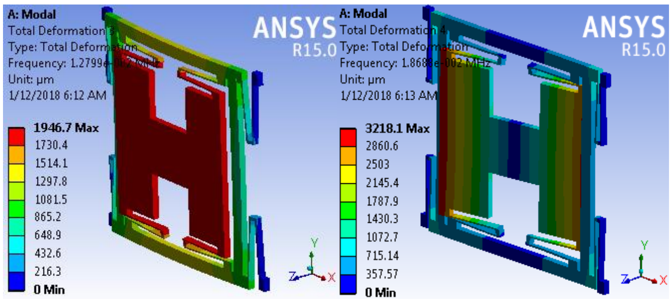

c) The parasitic modes

Figure 7: Some natural modes of the proposed MVG

The resonant frequencies of drive and sense modes are determined to be about 8.76 kHz and 9.09 kHz, respectively. This range of frequency ensures to reduce the effect of vibration and acoustic. In fact, the frequencies of two desired modes (drive and sense modes) should be matched to amplify the output signal on sense mode. But it may make a longer response time. Besides, when the difference between two modes is decreased, the mechanical coupling increases, which causes an increase the zero-rate output shift and the devise operation becomes more unstable [10], [11], [16]. The larger the range is, the quicker the response of sensor is. In this design, the bandwidth between the resonant drive and sense mode frequencies is 338 Hz (3.7%). This mismatched frequency is very large. The suitable value for mismatched frequency should be about 100 Hz to ensure the suitable bandwidth [21]. The frequency of the other modes, which are parasitic modes, is higher than two desired frequencies. This frequency is 12.799 kHz with third mode (bending mode), thus, there is a difference of about 41% between two low modes (sense and drive modes) and the higher modes. Thereby, it can reduce the crosstalk effect of parasitic frequencies in operating process.

The major frequencies strongly depend on the dimensions of structure. In order to match two wanted frequencies with supposed bandwidth, the investigation of relationship between the bandwidth (mismatched) frequency and the parameters of the structure should be carried out. In this paper, the authors focus on the length and width of the flexible beams in two directions. In this proposed structure, the width of the beams is designed to be much smaller than the thickness. The length and width is changed in range 450 ÷ 550 µm, 16 ÷ 22 µm and 440 ÷ 500 µm, 14 ÷ 20 µm for driving and sensing springs, respectively. The relationships between mismatched frequency and these parameters are determined in Response Surface ANSYS and shown in Figure 8. In each graph of Figure 8, two parameters are fixed, whereas two other are changed in the considered range. Moreover, it can be seen that the mismatched frequency strongly depends on the length of these beams. The widths of them affect complicatedly this frequency.

Table 4: The mismatched frequency corresponding to the specific value of folded beams

Driving spring		Sensing spring		Drive mode (Hz)	Sense mode (Hz)	Mism-atched (Hz)	Error %
Length (µm)	Width (µm)	Length (µm)	Width (µm)				
490	19	460	15	8396	8342	**54**	0.65
450	19	470	17	9467	9527	60	0.63
480	20	450	16	9266	9335	69	0.74
480	19	450	15	8647	8572	75	0.87
490	**20**	**460**	**16**	**8998**	**9098**	**100**	**1.1**
500	20	450	15	8743	8584	159	1.85
500	19	500	17	8178	8770	592	6.75

By using these results, we can determine the appropriate parameters for elastic beams with any desired mismatched frequency. The typical value of parameters can be consulted in Table 4. So, the minimum value of mismatched frequency is 54 Hz when the driving and sensing springs are about 490 µm, 460 µm for length and 19 µm, 15 µm for width, respectively. In order to have the 100 Hz bandwidth, the parameters should be chosen as 490 µm length, 20 µm width for driving beams and 460 µm length, 16 µm width for sensing beams, respectively. If the length of these beams is fixed, the width of them can be chosen from Figure 8 corresponding the desired mismatched frequency.

The above-chosen parameters are used to recalculate the characteristic value of system. Now, the equivalent stiffness coefficients in driving and sensing directions are respectively k_x = 1162 N/m and k_y = 769 N/m. In this case, the value of damping coefficient only includes slide damping of gas around system. Experimental data show that the effect of air damping is almost constant when the air pressure is near the atmospheric pressure. For example, the viscosity of air is 1.79×10^{-5} Ns/m at 1 atm and the viscosity reduces to 1.61×10^{-5} Ns/m at 0.5 atm

[22], [23]. Hence, the calculated frequencies of single gyroscope are ω_x = 8998 Hz and ω_y = 9098 Hz for drive mode and sense mode, respectively. The mismatched frequency is 100 Hz (1.1%). The next higher parasitic mode has further frequency (12931 Hz) with 42% difference from two lower modes. It means that the crosstalk effect can be suppressed and the amplitude along sensing direction achieves maximum [21].

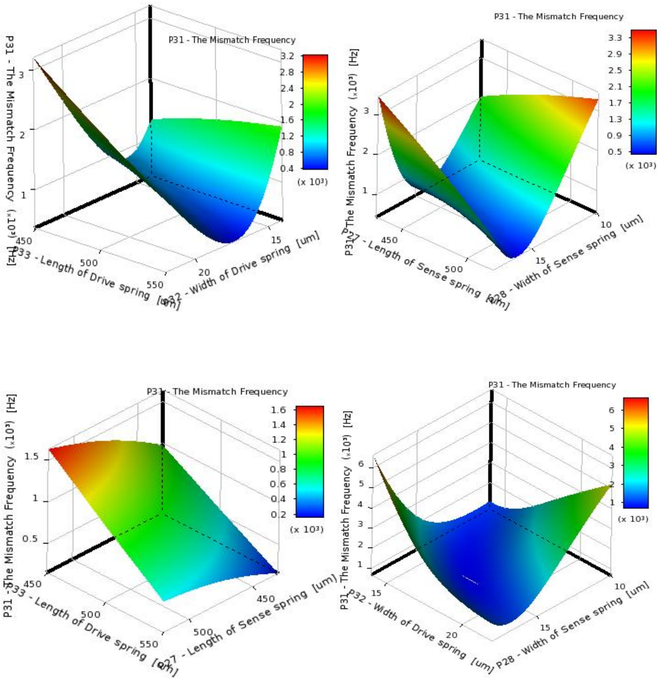

Figure 8: The effect of the dimension parameters of flexible beams to mismatched frequency

Amplitude-Frequency Response

When applying external force in drive direction, the desired response of gyroscope is that the drive vibration has stabilizing and maximum amplitude. It is necessary to determine the resonant frequency (*f*) of exciting force. The function of this force is defined as follow:

$$F = F_0 \sin(2\pi f t) \tag{19}$$

In order to determine this frequency, the amplitude of exciting force is fixed at F_0 = 1 μN, while the frequency *f* changes in range 8800 ÷ 9200 Hz to reduce the calculation time and ensure the calculation accuracy. The response of amplitude and phase to frequency is shown in Figure 9. Therefore, the resonant frequency is determined as 8998 Hz for drive oscillation and 9098 Hz for sense oscillation. These values are equal to the frequencies in modal analysis in ANSYS Workbench. So, the exciting frequency *f* could be defined as: *f* = 8998 Hz.

To compare with analytical method, according to expressions (15), (16) in above section, the resonant frequencies in driving and sensing directions are respectively 8968 Hz and 9085 Hz (Figure 10). The difference in two methods is negligible 0.33% and can be explained that the mass of flexible driving and sensing beams was not mentioned in analytical issue. Because of that the value of resonant frequencies in analytical method is slightly smaller than in simulation method. This result demonstrates that the analytical solution is fairy accurate.

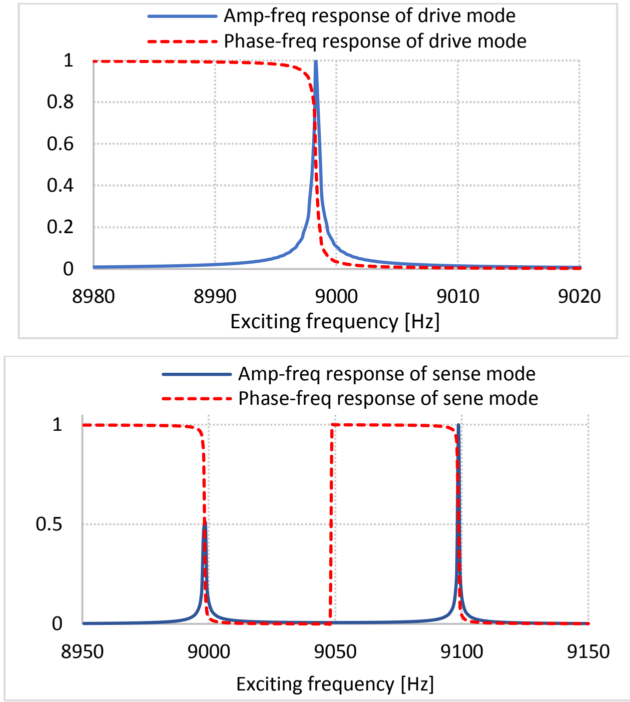

Figure 9: Simulated frequency responses

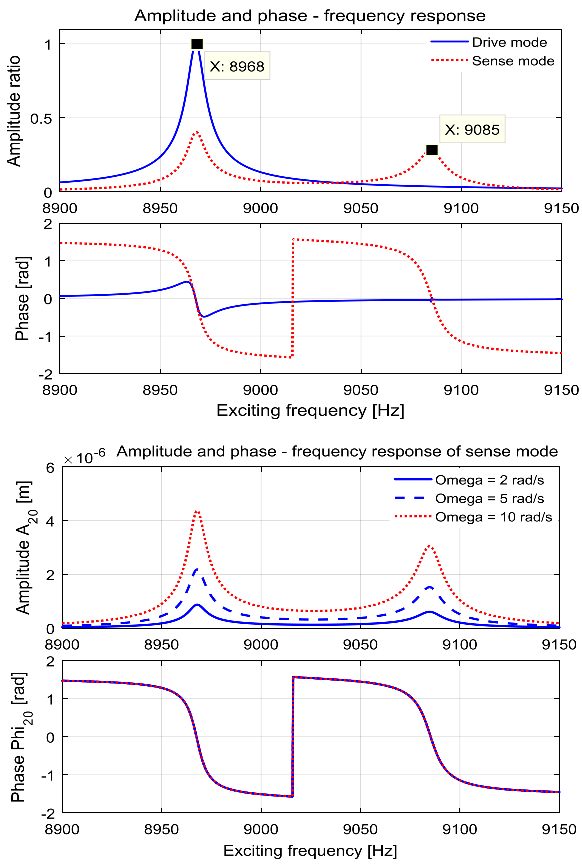

Figure 10: Analytical amplitude and phase responses versus exciting frequency

CONCLUSION

This paper presents a methodology to solve the dynamic analysis issue for a proposed two-degree-of-freedom MVG with two masses. In this MVG, the masses are connected together and to substrate by the U-shaped flexible beams. By using ANSYS Workbench software, the 3D and mesh model of this MVG is designed and then the modal analysis is carried out to define the frequency of two major modes of this gyroscope. The mismatched resonant frequency between these two modes is determined according to dimension parameters of U-shaped beams in two major directions. The equivalent stiffness coefficients of the flexible beams in sense and drive direction determined by both analytical and simulation method are matching with small errors as 3%. These values were used as the input parameter of the analytical problem. The frequency of drive and sense modes in both two methods were determined with slight error as 0.33%. The geometric parameters of U-shaped beams are optimized with the desired mismatched frequency as 100 Hz. The above obtained results are the basis to solve dynamic analysis issue for the single and double MVG in subsequent studies.

REFERENCES

[1] Cenk Acar, Andrei M. Shkel, MEMS Vibratory Gyroscopes - Structural Approaches to Improve Robustness, Springer, 2009.

[2] Yazdi N, Ayazi F and Najafi K, "Micromachined inertial sensors", Proceedings of the IEEE, 86, pp.1640-1659, 1998.

[3] Andrei M. Shkel, "Dynamics and control of micromachined gyroscopes", The American Control Conference, San Diego, California, pp. 2119-2124, 1999.

[4] Andrei M. Shkel, "Type I and type II micromachined vibratory gyroscopes", Proceedings of the IEEE/ION PLANS, SanDiego, USA, p. 586-592, 2006.

[5] Rana I. Shakoor, Shafaat Ahmed Bazaz, Michael Kraft, Yongjun Lai and Muhammad M. U Hassan, "Thermal Actuation Based 3-DoF on Resonant Microgyroscope Using MetalMUMPs", www.mdpi.com/journal, Sensors, Vol. 9, p. 2389-2414, 2009.

[6] Ralf Voss, Karin Bauer, Wilhelm Ficker, "Silicon angular rate sensor for automotive applications with piezoelectric drive and piezoresistive read-out", Proc. Transducers'97, Chicago, IL, pp. 879-882, 1997.

[7] Nan-Chyuan Tsai, Jiun-Sheng Liou, Chih-Che Lin, Tuan Li, "Design of Electromagnetic Drive Module for Micro-gyroscope", International Journal of Computer and Systems Engineering, Vol:4, No:10, p. 1534-1539, 2010.

[8] Andrei M. Shkel, Roberto Horowitz, "Dynamics and control of Micromachined Gyroscopes", Proceedings of the American Control Conference, pp. 2119-2124, 1999.

[9] Bumkyoo Choi, Seung-Yop Lee, Taekhyun Kim and Seog Soon Baek, "Dynamic characteristics of vertically coupled structures and the design of a decoupled micro-gyroscope", www.mdpi.com/journals, Sensors, vol.8, pp. 3706-3718, 2008.

[10] Said Emre Alper, Kivanc Azgin and Tayfun Akin, "A high-performance silicon-on-insulator MEMS gyroscope operating at atmospheric pressure", Sensors and Actuators A Physical, Vol.135, p. 34-42, 2007.

[11] Shady Sayed, Samer Wagdy, Ahmed Badawy, Moutaz M. Hegaze, "Symmetrical in-plane resonant gyroscope with decoupled modes", International Journal of Mechanical, Aerospace, Industrial, Mechatronic and Manufacturing Engineering, Vol. 11, No. 2, pp. 266-271, 2017.

[12] Dunzhu Xia, Cheng Yu and Lun Kong, "The Development of Micromachined Gyroscope Structure and Circuitry Technology", www.mdpi.com/journals, Sensors, Vol 14, 1394-1473, 2014.

[13] S. Emre Alper, T. Akin, "A symmetric surface micro-machined gyroscope with decouple oscillation modes", Sensors and Actuators A Physical, p. 347-358, 2002.

[14] Said Emre Alper and Tayfun Akin, "Symmetrical and decoupled nickel micro-gyroscope on insulating substrate", Sensors and Actuators, A Physical, p. 336-350, 2004.

[15] Said Emre Alper and Tayfun Akin, "A single-crystal silicon symmetrical and decoupled MEMS gyroscope on an insulating substrate", Journal of Microelectromechanical Systems, Vol. 14, No. 4, 2005.

[16] Ajit Sharma, Faisal M. Zaman, Babak V. Amini and Farrokh Ayazi, "A high-Q in-plane SOI tuning fork gyroscope", Proceedings of the IEEE 1, p. 467–470, 2004.

[17] Yanwei Guan · Shiqiao Gao · Lei Jin · Lianmin Cao, "Design and vibration sensitivity of a MEMS tuning fork gyroscope with anchored coupling mechanism", Microsyst Technol, Vol 22, p. 247–254, 2016.

[18] James J. Allen, Micro electromechanical system design, Taylor and Francis Group, 2005.

[19] Vladislav Apostolyuk and Francis E. H. Tay, "Dynamics of Micromechanical Coriolis Vibratory Gyroscopes", Sensor Letters, Vol.2, pp.1-8, 2005.

[20] I. Chowdhury and Shambhu P. Dasgupta, "Computation of Rayleigh Damping Coefficients for Large Systems", 2003.

[21] Marc S. Weinberg and Anthony Kourepenis, "Error sources in in-plane silicon tuning fork MeMS gyroscopes", Journal of Microelectromech Syst, 15 (3), p.479–491, 2006.

[22] Minhang Bao, Heng Yang, "Squeeze film air damping in MEMS", Science Direct, Sensors and Actuators, Vol. 136, p. 3-27, 2007.

[23] F. Pan, J. Kubby, E. Peeters, A. Tran, S.Mukherjee, "Squeeze film damping effect on the dynamic response of a MEMS torsion mirror", J. Micromechanical Microengineering, p. 200–208, 1998.